Opt Quant Electron (2015) 47:1347–1355
DOI 10.1007/s11082-014-0064-3

Design consideration of GaAs-based blocked-impurity-band detector with the absorbing layer formed by ion implantation

Xiaodong Wang · Bingbing Wang · Liwei Hou · Wei Xie · Xiaoyao Chen · Ming Pan

Received: 26 September 2014 / Accepted: 3 November 2014 / Published online: 15 November 2014
© Springer Science+Business Media New York 2014

Abstract Drawbacks and problems of the traditional liquid-phase-epitaxy grown mesa GaAs-based blocked-impurity-band (BIB) detector are discussed. In order to improve device performance, a novel planar GaAs-based BIB detector with the absorbing layer formed by ion implantation is proposed and modeled. Physical models and key parameters used for simulation are presented. Our results reveal that the transition region between the absorbing layer and the blocking layer can be as narrow as 3.125 μm by adopting the novel design. Bias-dependent electric field characteristics are then obtained by taking into account the immaturity of GaAs-based material. Temperature-dependent dark current characteristics are also simulated to investigate the impurity-band effect. Finally, the dependences of dark current and photoresponse on the thickness of the blocking layer are studied. It is demonstrated that the effective dark current suppression and sufficient photoresponse level can be realized by a proper control over the thickness of the blocking layer.

Keywords GaAs · Blocked-impurity-band (BIB) · Ion implantation · Blocking layer · Dark current · Photoresponse

1 Introduction

Terahertz (THz) wave is commonly known as electromagnetic radiation with wavelength ranging from 30 μm to 3 mm. Background-limited space-based THz detection is especially important for astronomical observations (Huffman et al. 1992). Moreover, space-based THz detection can achieve extremely high signal-to-noise ratio (Watson and Guptill 1993),

X. Wang (✉) · B. Wang · L. Hou · W. Xie · M. Pan
No. 50 Research Institute of China Electronics Technology Group Corporation,
318 Chang He Road, Shanghai 200331, China
e-mail: wxd06296@163.com

X. Chen
Laboratory of Advanced Material, Fudan University, Shanghai 200438, China

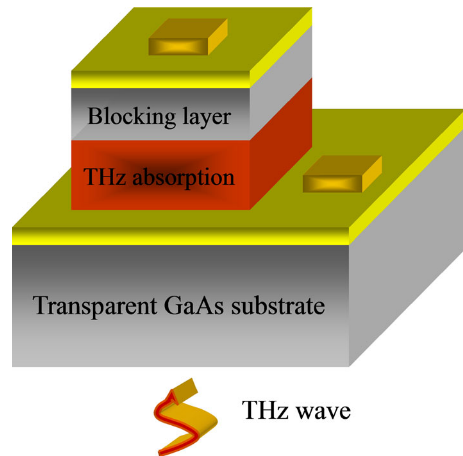

Fig. 1 3-D structure of traditional LPE grown mesa GaAs-based BIB detector

and has thus attracted a lot of attentions in the field of military applications including ballistic missile defense, and cool target tracking (Becker 2006).

Unlike room-temperature THz detectors (Guo et al. 2013; Hu et al. 2013a), space-based THz detectors pursue high sensitivity, high speed, and large format. The earliest space-based THz detector is bolometer, which has extremely high sensitivity all over the THz regime. However, long response time limits its wide applications. Subsequently developed THz detectors based on superconductor technology (e.g., HEB, SIS mixer, STJ detector, and TES) (Sizov and Rogalski 2010) had improved response speed significantly, and kept high sensitivity as well. But these superconducting devices still encounter several drawbacks including requiring complex cryocooler to achieve extreme temperature below 1 K, inconvenience to fabricate large-format arrays, and incompatibility with readout electronics. The above drawbacks can be overcome effectively by the blocked-impurity-band (BIB) detector, and thus high-performance space-based THz detection can also be realized by exploiting the BIB detector. In fact, because of its band gap tunability with x, $Hg_{1-x}Cd_xTe$ is also one of important and versatile materials for fabricating detectors operated at wave band ranging from the entire IR to THz regions under cryogenic temperature. However, due to the weak Hg–Te bond, which results in bulk, surface and interface instabilities, uniformity and yield become big issues, making HgCdTe detector less popular than BIB detector especially in LWIR and THz spectral range (Hu et al. 2014, 2013b).

Three classes of BIB detectors (Si-based, Ge-based, and GaAs-based) have been reported previously. Response wavelength of Si-based BIB detector can cover $2-40\,\mu$m range (Khalap and Hogue 2012). Ge-based BIB detector with the capability of extending response wavelength over 200 μm has been realized (Bandaru et al. 2002). GaAs-based BIB detector can further extend response wavelength beyond 300 μm, and has thus attracted extensive attentions since 2004 when the first prototype device was successfully developed in UC Berkeley (Cardozo 2004). Figure 1 presents the three-dimensional (3-D) structure of the traditional liquid-phase-epitaxy (LPE) grown mesa GaAs-based BIB detector (Reichertz et al. 2004; Haegel 2003). However, this structure is still facing several drawbacks and problems including: (1) the doping concentration of LPE grown GaAs can not be well controlled, and may vary by up to a factor of 3 about the targeted value, leading to poor device reproducibility; (2) a large number of impurities may be introduced into the blocking layer that is epitaxially grown on the absorbing layer, giving rise to large dark current;

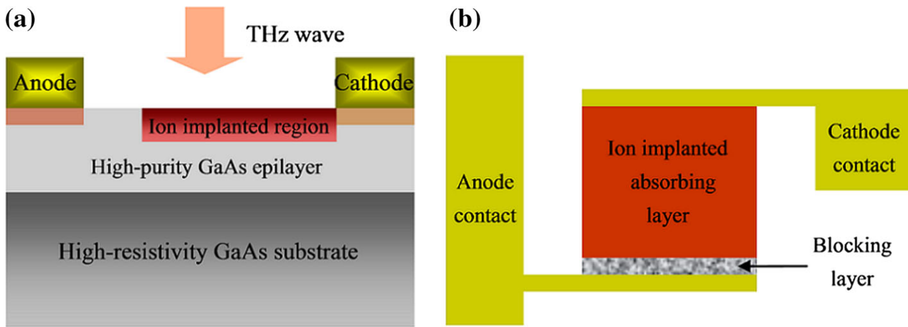

Fig. 2 **a** Cross-sectional view and **b** top view of planar GaAs-based BIB detector with the absorbing layer formed by ion implantation

(3) a high density of surface defects may appear during the mesa formation by etching process, causing not only larger dark current but also low responsivity. Besides, many groups have investigated electrical characteristics of Si-based and Ge-based BIB detectors (Haegel et al. 2000; Garcia and Haegel 2005; Liao et al. 2013), but few reports have been given to GaAs-based BIB devices due to its relatively immature material system and the lack of proper simulation methods to describe the effects of hopping conduction and impurity-band transition.

In order to overcome the above-mentioned drawbacks and problems encountered by the traditional GaAs-based BIB detector. As shown in Fig. 2, a novel planar GaAs-based BIB detector with the absorbing layer formed by ion implantation is proposed and modeled. The basic numerical models and parameters are described in Sect. 2. The advantages of the novel detector are discussed in Sect. 3 based on simulation results. Bias-dependent electric field characteristics are then obtained by taking into account the immaturity of GaAs-based material. Temperature-dependent dark current characteristics are also simulated to investigate the impurity-band effect. After that, the discussions focus on the role of the blocking layer in the optimization of device performance. Finally, conclusions are made in Sect. 4. The results would serve as a good sustentation for realization of novel high-performance THz detectors.

2 Device description and simulation models

The novel BIB detector area is $50 \times 50\,\mu\mathrm{m}^2$, and its structure consists of a $40\,\mu$m-thick absorbing layer and a $10\,\mu$m-thick blocking layer. Both layers are sandwiched between two metallic electrodes. The electrodes near the blocking layer and the absorbing layer are named as anode and cathode, respectively. The bias of cathode keeps 0 V during our simulation, and V_A denotes the forward bias applied between the anode and the cathode.

The two-dimensional numerical simulations were performed using Sentaurus Device, a commercial package by Synopsys (2008). The plain drift-diffusion model that couples Poisson equation and continuity equations is adopted. The carrier generation-recombination process consists of SRH, Radiative, and Auger terms (Wang et al. 2014). Theoretical expressions for all the above-mentioned physical models have been described elsewhere (Wang et al. 2011) in detail. High-field saturation model is selected for mobility calculation, and has the following form:

Table 1 Key parameters used in the simulation

Parameters (GaAs)	Units	Electron	Hole
Room-temperature bandgap E_g	eV	1.42	1.42
Dielectric constant ε_r		13.18	13.18
Density of states N	cm^{-3}	4.42×10^{17}	8.47×10^{18}
Effective mass (relative) m		0.067	0.481
Low-field mobility μ	cm^2/Vs	8500	400
SRH lifetime τ^{SRH}	sec	1×10^{-9}	1×10^{-9}
Radiative coefficient R^{Rad}	cm^3/s	2×10^{-10}	2×10^{-10}
Auger coefficient R^{Auger}	cm^6/s	1×10^{-30}	1×10^{-30}
High-field saturation A_{vsat}	cm/s	1.13×10^7	1.13×10^7
High-field saturation B_{vsat}	cm/s	3.6×10^6	3.6×10^6
High-field saturation $V_{sat,min}$	cm/s	5×10^5	5×10^5
High-field saturation β_0		2	2
High-field saturation β_{exp}		0	0

$$\mu(F) = \frac{\mu_{low}}{\left[1 + \left(\frac{\mu_{low} F}{v_{sat}}\right)^{\beta}\right]^{1/\beta}} \tag{1}$$

where μ_{low} denotes the low field mobility, and v_{sat} is given by:

$$v_{sat} = A_{vsat} - B_{vsat}\left(\frac{T}{T_0}\right) \text{ for } v_{sat} > v_{sat,min} \tag{2}$$

otherwise, $v_{sat} = v_{sat,min}$. The exponent β can be expressed as:

$$\beta = \beta_0 \left(\frac{T}{T_0}\right)^{\beta_{exp}} \tag{3}$$

Values of A_{vsat}, B_{vsat}, $V_{sat,min}$, β_0, and β_{exp} are listed in Table 1.

Additionally, incomplete ionization model is utilized for both donors and acceptors to represent the carrier freeze-out effect at low temperature. Since ion implantation technique possesses relatively low lateral diffusivity, we assume uniform doping for the blocking and absorbing layers with room-temperature donor (N_D) and acceptor (N_A) concentrations as follows:

$N_D = 1 \times 10^{12}\,cm^{-3}$, and $N_A = 1 \times 10^{11}\,cm^{-3}$ in the blocking layer;
$N_D = 5 \times 10^{15}\,cm^{-3}$, and $N_A = 5 \times 10^{12}\,cm^{-3}$ in the absorbing layer.

For simulations of electron density and dark current characteristics, the impurity-band effect is considered, and will be described in the following section. All of the key parameters can be found in Table 1.

3 Results and discussion

In this section, our discussion will focus on the electrical characteristics of GaAs:S BIB detector. Figure 3 shows the simulated contour map of electron density at $V_A = 0\,V$ and

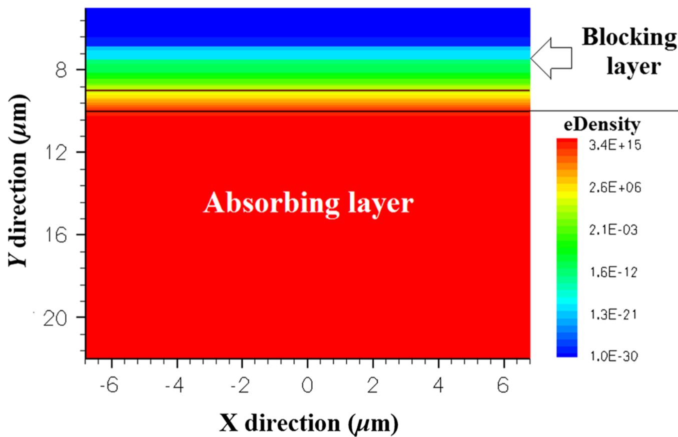

Fig. 3 Contour map of electron density for GaAs:S BIB detector at $V_A = 0\,\text{V}$ and $T = 15\,\text{K}$

$T = 15\,\text{K}$. As shown in Fig. 3, the 3.125μm-wide transition region between absorbing layer and blocking layer is formed due to electron diffusion. As for the traditional LPE grown mesa GaAs-based BIB detector at the same temperature, the width of transition region is much larger than 3.125 μm because additional dopants residual in the epitaxial reactor after the growth of absorbing layer will be unavoidably introduced into the blocking layer. The narrower transition region is favorable for the reduction of dark current and thus the suppression of thermal noise. This is one of the advantages of our novel design compared with the traditional scheme, and extra advantages include: (1) device reproducibility is improved because the doping concentration of the absorbing layer can be precisely controlled by ion implantation; (2) dark current is reduced because the blocking layer grown on the high-resistivity substrate exhibits much higher purity; (3) photoresponse is enhanced because planar technique can effectively avoid etching-induced surface defects.

Most of traditional numerical models for Si-based BIB devices are based on the assumption of charge neutrality in blocking layer, and thus the obtained electric-field intensity in this layer is uniform [e.g., (Garcia and Haegel 2005)]. However, the material quality of GaAs is not as mature as that of Si, and the number of impurities in GaAs is larger than that in Si. Therefore, the assumption mentioned above is not applicable to our GaAs-based BIB detector, and the traditional models need to be revised. As described in Sect. 2, it is assumed that the blocking layer has $N_D = 1 \times 10^{12}\,\text{cm}^{-3}$, and $N_A = 1 \times 10^{11}\,\text{cm}^{-3}$; the absorbing layer has $N_D = 5 \times 10^{15}\,\text{cm}^{-3}$, and $N_A = 5 \times 10^{12}\,\text{cm}^{-3}$. Figure 4 presents the simulated equilibrium electric-field distribution at $T = 5\,\text{K}$ using the revised device models. As shown in Fig. 4, the electric-field intensity in the blocking layer is a strong function of vertical position. The inset of Fig. 4 compares electric-field distributions with V_A changing from 0.45 to 0.95 V in 0.1 V steps. It is found that the space charge region extends from the blocker/absorber interface into the absorbing layer, and its width increases monotonically with the bias. The space charge region of GaAs:S BIB detector is also referred to as the depletion region where the ionized donors are depleted. This means that electrons excited by photons in the depletion region can travel along the bent conduction band, and then be directly collected by the anode without recombination at ionized donors. On the other hand, only the depletion region with high electric fields can drive the photo-generated electrons to the anode. Therefore, the width of the depletion region is extremely important for photoresponse, and a wider depletion region under higher bias will give rise to a larger photoresponse.

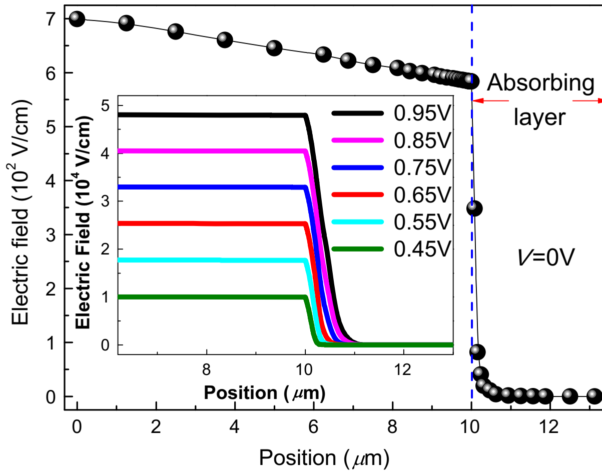

Fig. 4 Vertical electric-field distributions at different values of V_A, at $T = 5\,\text{K}$

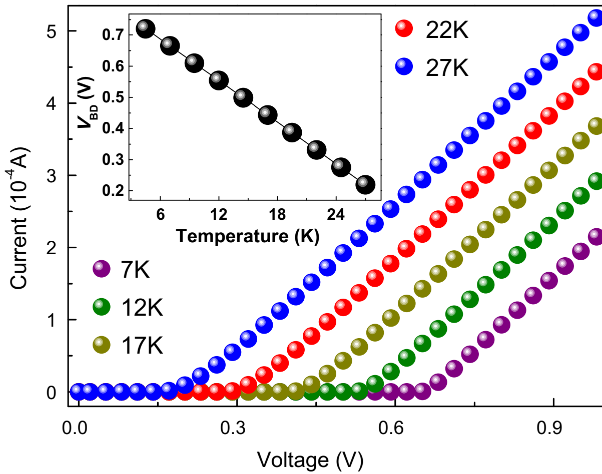

Fig. 5 Dark current characteristics of GaAs:S BIB detector at different temperatures. Inset shows the breakdown voltage as a function of temperature

Based on the revised numerical model above, temperature-dependent dark current characteristics are then simulated to investigate the impurity-band effect. It is known that dark current of GaAs:S BIB detector is dominated by two components. One is associated with thermally excited electrons from the impurity band to the conduction band, and the other is related to electrons hopping between impurity centers. Thus, constructing the impurity band that has proper energy gap with the conduction band is a critical step to simulate dark current characteristics. In our simulation, the role of impurity band is directly simulated by the valence band, and the bandgap is set to the excitation energy of S in GaAs (6 meV at 0 K). The obtained results are shown in Fig. 5. It is clear that the magnitude of dark current is very small if the bias is below a critical threshold value, but if the bias continues to increase, dark current will sharply rise. The phenomenon is attributed to the role of the blocking layer in the dark current suppression. The threshold voltage for a sharp rise of dark current corresponds to

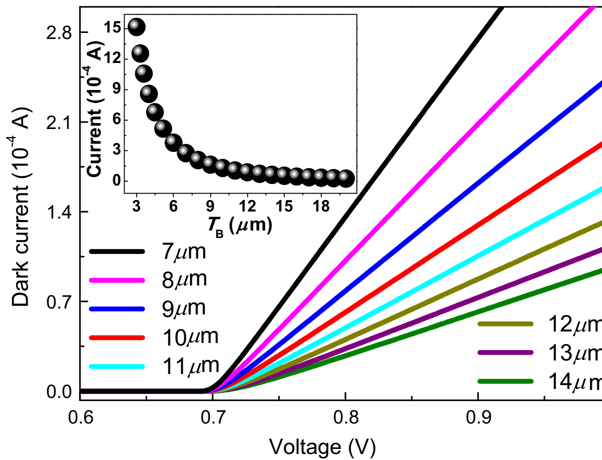

Fig. 6 Dark current characteristics of GaAs:S BIB detector for different values of T_B at $T = 5$ K. Inset shows dark current at 0.9 V bias versus T_B for $T = 5$ K.

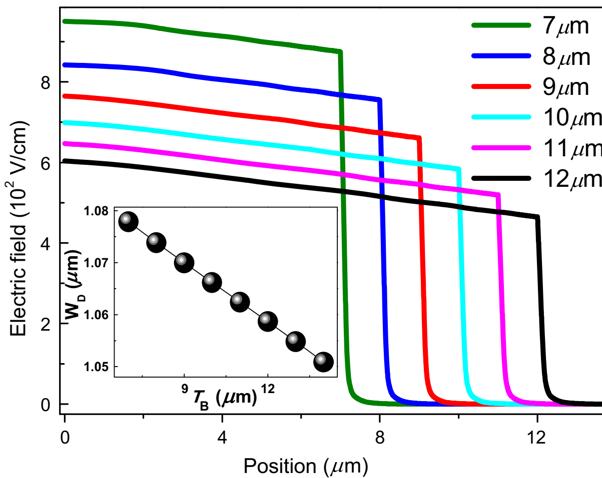

Fig. 7 Electric field characteristics of GaAs:S BIB detector for different values of T_B at $T = 5$ K. Inset shows the width of depletion region versus T_B for $T = 5$ K.

the electric breakdown of the blocking layer, and thus is also referred to as breakdown voltage (V_{BD}). According to the inset of Fig. 5, V_{BD} decreases linearly with increasing temperature, and the same trend has been observed in experimental results reported by the research group in UC Berkeley (Reichertz et al. 2005). The linear dependence of V_{BD} on temperature with a temperature coefficient of -0.0223 V/K is because an increase of temperature results in an enhanced thermal excitation of electrons from the impurity band to the conduction band, and thus the breakdown of the blocking layer at a decreased bias.

The thickness of blocking layer (T_B) as a key parameter of GaAs:S BIB detector possesses a significant influence on device performance. Therefore, an investigation on the effect of T_B on the dark current and photoreponse is necessary for optimizing device structure. Figure 6 compares Dark current characteristics of GaAs:S BIB detector for different values of T_B at

$T = 5\,\text{K}$. As indicated, T_B has a negligible influence on the dark current if $V_A < 0.7\,\text{V}$. However, if $V_A > 0.7\,\text{V}$, the situation is completely opposite. This means that the breakdown voltage of GaAs:S BIB detector is not a function of T_B possibly due to the immaturity of GaAs-based material. Inset of Fig. 6 shows the dark current at 0.9 V bias versus T_B for $T = 5\,\text{K}$. As observed, dark current first drops significantly with increasing T_B and then becomes saturated. For better comparison, Electric field characteristics of GaAs:S BIB detector are also investigated for different values of T_B at $T = 5\,\text{K}$. As shown in Fig. 7, an increase in T_B will give rise to an evident reduction in the electric-field intensity in the blocking layer. Additionally, if the width of the depletion region (W_D) is defined as the width from the blocker/absorber interface to the position where the electric-field intensity is equal to 1 V/cm, W_D as a function of T_B can be depicted in the inset of Fig. 7. It is noted that W_D decreases linearly with increasing T_B, which means that an increase in T_B will lead to a reduction in photoresponse. Taking the insets of both Figs. 6 and 7 into consideration, it is demonstrated that the effective dark current suppression and sufficient photoresponse level can be achieved at T_B of approximately 10 μm. This is because when T_B approaches 10 μm, the dark current is already close to the saturated value, and extra increase in T_B will contribute little to the suppression of thermal noise.

4 Conclusion

In this paper, a novel planar GaAs-based BIB detector with the absorbing layer formed by ion implantation has been proposed and modeled for overcoming disadvantages of the traditional LPE grown GaAs-based BIB detector including poor reproducibility, large dark current, and low responsivity. Our results reveal that the transition region between the absorbing layer and the blocking layer can be as narrow as 3.125 μm by adopting the novel design. Bias-dependent electric field characteristics have also been obtained by taking into account the immaturity of GaAs-based material. It is found that the space charge region extends from the blocker/absorber interface into the absorbing layer, and its width increases monotonically with the bias. The linear dependence of V_{BD} on temperature with a temperature coefficient of -0.0223 V/K is obtained by coupling the impurity-band effect into our numerical models. Furthermore, it is demonstrated that the effective dark current suppression and an acceptable photoresponse level can be achieved at T_B of approximately 10 μm.

Acknowledgments This work was supported by the National Natural Science Foundation of China (Grant No. 61404120).

References

Bandaru, J., Beeman, J.W., Haller, E.E.: Far-infrared absorption in Sb-doped Ge epilayers near the metal-insular transition. Appl. Phys. Lett. **80**, 3536–3538 (2002)

Becker, L.: Influence of IR sensor technology on the military and civil defense. Proc. SPIE 6127, 61270S-1-15 (2006)

Cardozo, B.L.: GaAs blocked-impurity-band detectors for Far-Infrared astronomy. Doctoral thesis. University of California, Berkeley (2004)

Garcia, J.C., Haegel, N.M.: Alternate operating mode for long wavelength blocked impurity band detectors. Appl. Phys. Lett. 87, 043502-1-3 (2005)

Guo, N., Hu, W.D., Chen, X.S., Wang, L., Lu, W.: Enhanced plasmonic resonant excitation in a grating gated field-effect transistor with supplemental gates. Opt. Express **21**, 1606–1614 (2013)

Haegel, N.M., Jacobs, J.E., White, A.M.: Modeling of steady-state field distributions in blocked impurity band detectors. Appl. Phys. Lett. **77**, 4389–4391 (2000)
Haegel, N.M.: BIB detector development for the far infrared: from Ge to GaAs. Proc. SPIE **4999**, 182–194 (2003)
Hu, W., Chen, X., Ye, Z., Feng, A. L., Yin, F., Zhang, B., Liao, L., and Lu, W.: Dependence of ion-implant-induced LBIC novel characteristic on excitation intensity for Long-wavelength HgCdTe-based Photovoltaic Infrared Detector Pixel Arrays, IEEE J. Sel. Top. Quantum Electron. 19, 4100107-1-7 (2013b)
Hu, W.D., Wang, L., Chen, X.S., Guo, N., Miao, J.S., Yu, A.Q., Lu, W.: Room-Temperature Plasmonic Resonant Absorption for Grating-gate GaN HEMTs in far infrared terahertz domain. Opt. Quantum Electron. **45**, 713–720 (2013a)
Hu, W., Ye, Z., Liao, L., Chen, H., Chen, L., Ding, R., He, L., Chen, X., Lu, W.: A 128 $\times$ 128 long-wavelength/mid-wavelength two-color HgCdTe infrared focal plane array detector with ultra-low spectral crosstalk. Opt. Lett. **39**, 5184–5187 (2014)
Huffman, J.E., Crouse, A.G., Halleck, B.L., Downes, T.V.: Si:Sb blocked impurity band detectors for infrared astronomy. J. Appl. Phys. **72**, 273–275 (1992)
Khalap, V., Hogue, H.: Antimony doped silicon blocked impurity band (BIB) arrays for low flux applications. Proc. SPIE 8512, 85120O-1-7 (2012)
Liao, K.S., Li, N., Liu, X.H., Huang, L., Zeng, Q.Y., Zhou, X.H., Li, Z.F.: Ion-implanted Si: P blocked-impurity-band photodetectors for far-infrared and terahertz radiation detection. Proc. SPIE 8909, 890913-1-9 (2013)
Reichertz, L.A., Cardozo, B.L., Beeman, J.W., Larsen, D.I., Tschanz, S., Jakob, G., Katterloher, R., Haegel, N.M., Haller, E.E.: First results on GaAs blocked impurity band (BIB) structures for far-infrared detector arras. Proc. SPIE 5883, 58830Q-1-8 (2005)
Reichertz, L.A., Beeman, J.W., Cardozo, B.L., Haegel, N.M., Haller, E.E., Jakob, G., Katterloher, R.: GaAs BIB photodetector development for far-infrared astronomy. Proc. SPIE **5543**, 231–238 (2004)
Sizov, F., Rogalski, A.: THz detectors. Prog. Quantum Electron. **34**, 278–347 (2010)
Synopsys: Sentaurus Device User Guide, Synopsys Inc., USA (2008)
Wang, X.D., Hu, W.D., Pan, M., Hou, L.W., Xie, W., Xu, J.T., Li, X.Y., Chen, X.S., Lu, W.: Study of gain and photoresponse characteristics for back-illuminated separate absorption and multiplication GaN avalanche photodiodes. J. Appl. Phys. 115, 013103-1-8 (2014)
Wang, X.D., Hu, W.D., Chen, X.S., Xu, J.T., Li, X.Y., Lu, W.: Photoresponse study of visible blind GaN/AlGaN p-i-n ultraviolet photodetector. Opt. Quantum Electron. **42**, 755–764 (2011)
Watson, D.M., Guptill, M.T.: Germanium blocked-impurity-band detector arrays: unpassivated devices with bulk substrates. J. Appl. Phys. **74**, 4199–4206 (1993)